Indian Journal of Pure & Applied Physics
Vol. 57, May 2019, pp. 293-301

Effects of radiation and chemical reaction on convective nanofluid flow through a non-linear permeable stretching sheet with partial slip

G Sreedevi*

Department of Mathematics, ASR College of Engineering, ASR Group of Educational Institutions, Tanuku 534 218, India

Received 10 October 2018; accepted 29 January 2019

The steady, convective two-dimensional nanofluid flow has been investigated under the influence of radiation absorption and chemical reaction through a porous medium. The flow has been caused by a non-linear stretching sheet with the slip effects of the velocity, the temperature and the nanoparticle concentration. The fluid is electrically conducted in the presence of an applied magnetic field. Appropriate transformations reduce the non-linear partial differential system to an ordinary differential system. The convergent solutions of the governing non-linear problems have been computed using fifth-order-Runge-Kutta-Fehlberg integration scheme. The results of the velocity, the temperature, and the concentration fields have been calculated in series forms. The effects of the different parameters on the velocity, the temperature, and the concentration profiles are shown and analyzed. The skin friction coefficient, the Nusselt and the Sherwood numbers have also been computed and investigated for different embedded parameters in the problem statement.

Keywords: Nanofluid, Non-linear stretching sheet, Slip effect, Radiation absorption,Chemical reaction

1 Introduction

The vital heat transfer limitation of conventional fluids, such as water, oil, ethylene glycol, over metallic and non-metallic materials has led to the innovation of improvement in the enhancement of heat transfer by combining together a homogeneous mixture of nano-scale particles (1-100 nm) and base fluids, which was coined as nanofluids by Choi[1]. The thermal radiation interaction with nanofluid flow is very important for various industrial and engineering applications because of the manner in which radiant emission depends on temperature and nanoparticles volume fraction (Brewster)[2]. The imperative foundation of a nanofluid is an agglomerate stable suspension for extended durations without triggering chemical changes in the base fluid. This can be accomplished by limiting the density amongst solids and fluids or by expanding the viscosity of the liquid explained by Kuznetsov and Nield[3]. Specially, the heat transfer coefficient intensifies to act to go beyond the mere thermal-conductivity effect, and cannot be predicted by Dittus-Boelter's traditional pure-fluid. Buongiorno[4] recommended a model for better understanding of the heat transfer augmentation with asymmetrical convective nanofluids and removed the flaws of the dispersion and homogenous models. He also studied seven slip systems, including Brownian diffusion, inertia, thermophoresis, diffusion-phoresis, magnus and gravity. He proved with his observations that only Brownian diffusion and thermophoresis are predominant slip mechanisms in nanofluids. Many investigators, Khan and Pop[5], Gorder *et al.*[6], Hassan *et al.*[7], Akyildiz[8], Rana and Bhargava[9] explored the boundary layer flow and heat transfer of nanofluid past non-linear stretching sheet by assuming the increase in nanofluids thermal conductivity abnormally and brownian motions of the nanoparticles inside the base fluids employing various mathematical and numerical modelling techniques. The flow of nanoparticles over a non-linear permeable stretching sheet with partial slip has been studied by Kalidas Das[10], Sreedevi*et al.*[11,12] Makinde and Animasaun[13] have studied the radiant emission which depends on temperature and nanoparticles volume fraction past linear stretching sheet. Sreedevi *et al.*[14,15] have numerically analysed the heat and mass transfer of nanofluid flow past both linear and non-linear stretching sheets with thermal radiation and chemical reaction by employing Galerkin finite element method. Jahan *et al.*[16] have observed that the Brownian motion effect becomes negligible and the local Nusselt number is almost independent of the Brownian motion while heat transfer reduces with Lewis number and thermophoresis parameter. Reddy

*E-mail: sreedevihari2007@gmail.com

et al.[17] have observed the effects of magnetic field, chemical reaction in presence of suction/ injection on MHD boundary layer flow of nanofluids and heat transfer over a non-linear stretching sheet by employing Keller box method.

The study of magnetohydrodynamic mixed convection nanofluid flow over a non-linear stretching sheet is significant for many applications in the field of chemical engineering (polymer technology, glass fiber production, paper production, manufacturing of plastic, rubber sheets, manufacture of foods, liquid films in condensation process) and metallurgical processes (metal and non-metallic extrusion procedure, drawing of plastic films and wires and crystal growing). Sakiadis[18] has investigated the flow of laminar boundary layer function on a moving continuous flat surface by two methods. Crane[19] considered in his work, the boundary layer flow near a stagnation point in which the main velocity in the outer flow is proportional to the distance from the stagnation point. Schlichting[20], Grubka and Bobba[21], Cortell[22], Ishak *et al.*[23], Wang[24] and Abbasbandy *et al.*[25] have explored the heat transfer and boundary layer flow past unsteady/continuous moving permeable stretching sheet with variable temperature and surface slip. Noghrehabadi *et al.*[26] studied the partial slip. The magnetohydrodynamic mixed convective flow over a permeable non-isothermal wedge has been studied by Prasad *et al*.[27] Further, Goyal and Bhargava[28], Cortell[29], Sheikholeslami *et al.*[30], Khalili *et al*.[31] have extended their study on boundary layer nanofluid flow and heat transfer past non-linear stretching sheet in porous medium. Zaimi *et al*.[32] numerically studied the magneto hydrodynamic flow, heat, and mass transfer of a nanofluid through a porous medium over a non-linear stretching sheet with slip conditions. Seth *et al.*[33] analysed the effects of viscous dissipation and thermal radiation on MHD flow past a non-linear stretching surface. Hayat *et al*.[34] and Mabood *et al.*[35] have discussed heat and mass transfer phenomena on electrically incompressible viscous, boundary layer flow of nanofluids past non-linearly stretching surface with slip effects. Seth *et al*.[36] have observed the effect of Joule dissipation, heat absorbing and radiating hydromagnetic fluid flow over exponentially stretching surface with partial slip.

Motivated by the above investigations and possible applications, this paper is devoted to examine the convective nanofluid flow through a non-linear permeable stretching sheet with partial slip in the presence of radiation and chemical reaction. The system of ordinary coupled equations is reduced into simultaneous equations and these equations are solved by using fifth order Runge-Kutta-Fehlberg integration scheme with automatic grid generation scheme which ensures convergence at a faster rate. The effect of several parametric values on the velocity, temperature, nanoparticle concentration, heat and mass transfer characteristics of the fluid flow are analysed.

2 Problem Formulation

Let us consider, the steady, convective, incompressible two-dimensional boundary layer and heat and mass transfer flow of electrically conducted nanofluid past a non-linear stretching surface with combined effect of radiation absorption and chemical reaction in a porous medium. It is assumed that the x-axis is taken along the stretching surface in the motion direction and the y-axis is perpendicular to it. A transverse magnetic field $H = H_0 x^{\frac{n-1}{2}}$ acts in a transverse direction to the flow. A Cartesian rectangular co-ordinate system O (x, y) is considered with the plate in the y-direction and x-axis normal to the boundary. The sheet is located at y=0 and its leading edge is the origin of the Cartesian coordinate system. The external electric field assumed to be zero and the magnetic Reynolds number is assumed to be small. Hence, the induced magnetic field is small compared with the external magnetic field. The effects of the Brownian motion and thermophoresis are presented. The boundary layer flow is governed by the following equations:

Continuity equation $$\frac{\partial u}{\partial x} + \frac{\partial v}{\partial y} = 0 \qquad \ldots (1)$$

Momentum equation

$$u\frac{\partial u}{\partial x} + v\frac{\partial u}{\partial y} = \nu\frac{\partial^2 u}{\partial y^2} - \frac{\sigma H^2 u}{\rho} - \left(\frac{\mu}{k}\right)u + \rho_f g(1-\varphi_\infty)\beta_T(T-T_\infty) - (\rho_p - \rho_{f\infty})g(\varphi-\varphi_\infty) \qquad \ldots (2)$$

Energy equation

$$u\frac{\partial T}{\partial x} + v\frac{\partial T}{\partial y} = \alpha\frac{\partial^2 T}{\partial y^2} + \tau\left(D_B\frac{\partial T}{\partial y}\frac{\partial C}{\partial y} + \frac{D_T}{T_\infty}\left(\frac{\partial T}{\partial y}\right)^2\right) + Q_H(T-T_\infty) - \frac{\partial q_r}{\partial y}\left(\frac{1}{(\rho C_p)_f}\right) \qquad \ldots (3)$$

Concentration equation

$$u\frac{\partial C}{\partial x} + v\frac{\partial C}{\partial y} = D_B\frac{\partial^2 C}{\partial y^2} + \left(\frac{\partial^2 T}{\partial y^2}\right)\frac{D_T}{T_\infty} - Kr(C - C_\infty) \qquad \ldots (4)$$

Following Hayat *et al.*[34] the boundary conditions for the velocity, temperature and nanoparticle concentration are as follows:

$$u = ax^n + \beta_1 \frac{\partial w}{\partial y}.\ v = 0,\ T = T_W + \beta_2 \frac{\partial T}{\partial y},\quad C = C_W + \beta_3 \frac{\partial C}{\partial y},\ \ at\ \ y = 0,$$
$$u \to 0,\qquad T \to T_\infty,\qquad C \to C_\infty \qquad as \qquad y \to \infty \qquad \ldots (5)$$

In the above equations, u and v are the velocity components along the x and y-directions. T, T_∞, C, C_∞, n, v, ρ, σ are the fluid temperature, the ambient fluid temperature, the constant wall concentration, the nanofluid concentration, power-law index, the kinematic viscosity, the density, the electrical conductivity of the fluid, respectively. $\tau = (\rho C)_p / (\rho C)_f, D_B$, D_T are the ratio of the effective heat capacity of the nanoparticle material to the heat capacity of the fluid, Brownian diffusion coefficient, thermophoretic diffusion coefficient, $\alpha = k/(\rho C_p)_f$ is the thermal diffusivity, β_1, β_2,β_3 are the slip constant, thermal slip parameter and concentration slip parameter, respectively. η, γ are the similarity variable and local slip parameter. It is assumed that the surface is stretched with velocity $u = ax^n f'(n)$, where a>0 is a constant.Introducing the following similarity transformations:

$$u = ax^n f'(n).\ v = -\sqrt{\frac{va(n+1)}{2}} x^{\frac{n-1}{2}} \left(f(\eta) + \frac{n-1}{n+1} \eta f'(\eta) \right),$$
$$\eta = \sqrt{\frac{a(n+1)}{2v}} x^{\frac{n-1}{2}} y,\ \ \theta(\eta) = \frac{T - T_\infty}{T_W - T_\infty},\qquad \phi(\eta) = \frac{C - C_\infty}{C_W - C_\infty}, \qquad \ldots (6)$$

Now, Eq. (1) is satisfied automatically and the partial differential Eqs (2) and (5) are converted into the non-linear, coupled and ordinary differential equations after using Eq. (6) can be reduced as follows:

$$f''' + ff'' - \frac{2n}{n+1} f'^2 - (M + D^{-1}) f' + Gr(\theta - Nr\phi) = 0 \qquad \ldots (7)$$

$$(1 + \frac{4Rd}{3}) \frac{1}{Pr} \theta'' + f\theta' + N_b \theta'\phi' + N_t \theta'^2 + Q\theta = 0 \qquad \ldots (8)$$

$$\phi'' + Lef\phi' + (\frac{N_t}{N_b})\theta'' - Kr\phi = 0 \qquad \ldots (9)$$

$$f'(0) = 1 + \gamma f''(0),\qquad f(0) = 0,\qquad \theta(0) = 1 + \delta\theta'(0)$$
$$\phi(0) = 1 + \varepsilon\phi'(0),\qquad f'(\infty) = 0,\qquad \theta(\infty) = 0,\qquad \phi(\infty) = 0 \qquad \ldots (10)$$

Where,

$M = \frac{\sigma H_0^2}{\rho a}$	Hartmann number	$N_t = \frac{\tau D_T (T_w - T_\infty)}{T_\infty \nu}$	Thermophoresis parameter
$Gr = \frac{\beta_T g \rho_{f\infty} (1-\phi_\infty)(T_W - T_\infty)}{(ax^n)^2}$	local Grash of number	$Le = \frac{\nu}{D_B}$	Lewis number
$Pr = \frac{\mu C_p}{K_f}$	Prandtl number	$Kr = \frac{2K_r' x}{ax^n(n+1)}$	Chemical reaction parameter
$Rd = \frac{4\sigma^* T_\infty^3}{\beta_R K_f}$	Radiation parameter	$\gamma = \beta_1 \sqrt{\frac{a(n+1)}{2\nu}} x^{\frac{n-1}{2}}$	Local slip parameter
$N_b = \frac{\tau D_B (C_w - C_\infty)}{\nu}$	Brownian motion parameter	$\varepsilon = \beta_3 \sqrt{\frac{a(n+1)}{2\nu}} x^{\frac{n-1}{2}}$	Local concentration slip parameter
$\delta = \beta_2 \sqrt{\frac{a(n+1)}{2\nu}} x^{\frac{n-1}{2}}$	Local thermal slip parameter	$D^{-1} = \frac{\nu x}{akx^n}$	Inverse Darcy parameter
$Q = \frac{2Q_H x}{ax^n(n+1)}$	Heat source parameter		

The important interested physical quantities in this problem are the local skin-friction coefficient C_f, the local Nusselt number Nu, and local Sherwood number Sh, which are defined by:

Local Skin friction

$$C_f = \frac{\tau_w}{\rho u_w^2}$$

It is clear that the wall shear stress will increase with increasing x. The skin friction coefficient C_f takes the form as:

$$C_f (Re_x)^{1/2} = \sqrt{\frac{n+1}{2}} f''(0) \qquad \ldots (11)$$

Local Nusselt number

$$Nu = \frac{x q_w}{k(T_w - T_\infty)}$$

Using the above equation, the local Nusselt number takes the form as:

$$Nu_x(Re_x)^{-1/2} = -\sqrt{\frac{n+1}{2}}\,\theta'(0) \quad \ldots (12)$$

Local Sherwood number

$$Sh = \frac{xh_m}{D_B(C_w - C_\infty)}$$

Simplifying the above equation, it takes the form as:

$$Sh_x(Re_x)^{-1/2} = -\sqrt{\frac{n+1}{2}}\,\phi'(0) \quad \ldots (13)$$

Where,

$$\tau_w = \mu\left.\frac{\partial w}{\partial y}\right|_{y=0}, \quad q_w = -k\left.\frac{\partial T}{\partial y}\right|_{y=0}, h_m = -D_B\left.\frac{\partial C}{\partial y}\right|_{y=0}$$

$Re_x = u_w\, x/\nu$ is the local Reynolds number.

3 Numerical Procedures

The coupled ordinary differential Eqs (7-9) are of third order in f and second order in θ and ϕ which have been reduced to a system of nine simultaneous equations of first-order for nine unknowns. In order to solve this system of equations numerically requires nine initial conditions but two initial conditions on f and one initial condition each on θ and ϕ are known. However, the values of f', θ and ϕ are known at $\eta \to \infty$. These three end conditions are utilized to produce four unknown initial conditions at η=0 by using shooting technique. The most crucial factor of this scheme is to choose the appropriate finite value of η_∞. In order to estimate the value of η_∞, start with some initial guess value and solve the boundary value problem consisting of Eqs (7–9) to obtain $f''(0)$, $\theta'(0)$ and $\phi'(0)$. The solution process is repeated with another large value of η_∞ until two successive values of f'' (0), θ′ (0) and ϕ′ (0) differ only after desired significant digit. The last value of η_∞ is taken as the final value of η_∞ for a particular set of physical parameters for determining velocity components $f'(\eta)$, temperature $\theta(\eta)$ and concentration $\phi(\eta)$ in the boundary layer. After knowing all the nine initial conditions, the system of simultaneous equations are solved. For faster convergence of the equations, fifth order Runge-Kutta-Fehlberg integration scheme with automatic grid generation is adopted in the present paper. The value of η_∞ greatly depends also on the set of the physical parameters, so that no numerical oscillations would occur. During the computation, the shooting error was controlled by keeping it to be less than 10^{-6}. Thus, the coupled non-linear boundary value problem of third order in f, second order in θ and ϕ has been reduced to a system of nine simultaneous equations of first-order for nine unknowns as follows :

$$f_1 = f, f_1^1 = f_2, \quad f_2^1 = f_3, f_4 = \theta, f_4^1 = f_5, f_6 = \phi, f_6^1 = f_7, \quad \ldots (14)$$

$$f_3^1 = -f_1 f_3 + (\frac{2n}{n+1}) f_2^2 + (M + D^{-1}) f_2 - Gr(f_4 - Nrf_6) \quad \ldots (15)$$

$$f_5^1 = [-3\,\mathrm{Pr}(\frac{f_7}{3+4Rd}) - f_1 f_5 + N_b f_5 f_7 + N_t f_5^2 + Qf_4] \quad \ldots (16)$$

$$f_7^1 = -Lef_1 f_7 - (N_t/N_b)[-3\mathrm{Pr}(\frac{f_7}{3+4Rd}) - f_1 f_5 + N_b f_5 f_7 + N_t f_5^2 + Qf_4] + Krf_6 \quad \ldots (17)$$

The prime differentiation with respect to η and the boundary conditions become as:

$$\left.\begin{aligned} f_2 = 1 + \eta\, f_3, \;\; f_4 = 1 + \delta\, f_5, \;\; f_6 = 1 + \varepsilon\, f_7 \qquad at \quad \eta = 0 \\ f_2 \to 0, \;\; f_4 \to 0, \;\; f_6 \to 0 \qquad at \quad \eta \to \infty \end{aligned}\right\} \quad \ldots (18)$$

Since, f_3 (0), f_5 (0), f_7 (0) are not prescribed so, to start with the initial approximations as f_3 (0) =s_{10}, f_5 (0) =s_{20}, f_7 (0) =s_{30}. Let γ_1, γ_2, γ_3 be the correct values of f_3 (0), f_5 (0) and f_7 (0), respectively. The resultant system of nine ordinary differential equations is integrated using fifth order Runge-Kutta-Fehlberg method and denote the values of f_3, f_5, f_7 at $\eta = \eta_\infty$ by $f_3(s_{10}, s_{20}, s_{30}, s_{40}), f_5(s_{10}, s_{20}, s_{30}, s_{40,}\eta_\infty), f_7(s_{10}, s_{20}, s_{30}, s_{40,}\eta_\infty)$, respectively. Since, f_3, f_5,f_7 at $\eta = \eta_\infty$ are clearly function of γ_1, $\gamma_{2,}$ γ_3 they are expanded in Taylor series around $\gamma_1 - s_{10}$, $\gamma_2 - s_{20}$, $\gamma 3 - s_{30}$, respectively by retaining only the linear terms. The use of difference quotients is made for the derivatives appeared in these Taylor series expansions. Thus,

after solving the system of Taylor series expansions for $\delta\gamma_1 = \gamma_1 - s_{10}$, $\delta\gamma_2 = \gamma_2 - s_{20}$, $\delta\gamma_3 = \gamma_3 - s_{30}$, the new estimates $s_{11}=s_{10}+\delta s_{10}$, $s_{21}= s_{20}+\delta s_{20}$, $s_{31}=s_{30}+\delta s_{30}$. Next the entire process is repeated starting with f_1 (0), f_2 (0), s_{11}, f_4 (0), s_{21}, s_{31} as initial conditions. Iteration of the whole outlined process is repeated with the latest estimates of γ_1, γ_2, γ_3 and γ_4 until prescribed boundary conditions are satisfied. Finally, $s_{1n}=s_{1(n-1)}+ \delta\ s_{1(n-1)}$, $s_{2n}=s_{2(n-1)}+ \delta\ s_{2(n-1)}$,$s_{3n}=s_{3(n-1)}+\delta\ s_{3(n-1)}$ and $s_{4n}=s_{4(n-1)}+\delta\ s_{4(n-1)}$ for n=1,2,3,... are obtained which seemed to be the most desired approximate initial values of $f_3(0)$, $f_5(0)$, $f_7(0)$ and in this way all the six initial conditions are determined. Now it is possible to solve the resultant system of seven simultaneous equations by fifth order Runge-Kutta-Fehlberg integration scheme so that velocity, temperature fields and nanoparticle volume fraction for a particular set of physical parameters can easily be obtained. The results are provided in several graphs.

4 Comparison

In the absence of Grashof number Gr, magnetic effect M, chemical reaction effect kr, radiation absorption Rd, heat source parameter Q, inverse Darcy parameter D^{-1} and buoyancy ratio Nr, the results obtained herein are compared with Das[10] and Cortell[29]. Further, in the absence of Gr, Q, Kr, Rd, D^{-1}, Nrfor different values of N_t, N_b, the results obtained herein are compared with the rate of heat and mass transfer coefficients with those of Goyal, Bhargava[28] and Hayat[34] for their nanofluid flow case. The above comparisons are shown in Table 1 and Table 2 and the results are found to be in excellent agreement.

5 Results and Discussion

Numerical solutions to governing non-linear coupled ordinary differential Eqs (14-17) with boundary condition Eq. (18) have no closed-form solution. Thus, these equations are solved numerically using the Runge–Kutta–Fehlberg method with shooting technique. Here the impact of buoyancy ratio parameter Nr, radiation absorption Rd, chemical reaction Kr and Prandtl number Pr on velocity, temperature, concentration, skinfriction, Nusselt number and Sherwood number are addressed through the graphs Figs 2-11 with non-linear stretching parameter n. Figures 2-7 represent the velocity, temperature and nanoparticle concentration profiles for various values of parameter. It is seen that all of these figures satisfy the boundary conditions (Eq.18).

5.1 Velocity profiles

Figure 2 illustrates the impact of Nr and Rd parameters. It can be seen from the profiles that the boundary layer thickness and the velocity enhance with increase in the values of Nr, Rd and n. This is because, an increase in convection results in a growth of thermal buoyancy force which is responsible for higher velocity. Figure 3 represents the effect of Kr and Pr on the velocity profile. An increase

Table 1 – Comparison of Nusselt number Nu for Gr=M=Kr=Rd=Q=D^{-1}=Nr=0, case with different Pr with Das[10] and Cortell[29].

Pr	Das[10]	Cortell[29]	Present results
	Nu	Nu	Nu
0.71	0.678327	0.654327	0.667389
1.71	0.623256	0.640373	0.6243524
3.71	0.603424	0.629174	0.604334
6.2	0.586724	0.605424	0.5876032

Table 2 – Comparison of heat and mass transfer with Goyal and Bhargava[28] for Gr=Kr=Rd=D^{-1}=Nr=0 and Hayat *et al.* [34] for Gr=Kr=Q=Rd=D^{-1}=Nr=0 of their nanofluid flow case for different values of N_t, N_b.

N_t	N_b	Goyal and Bhargava[28]		Present results		Hayat *et al*.[34]		Present results	
		Nu	Sh	Nu	Sh	Nu	Sh	Nu	Sh
0.1	0.1	0.95243	2.12936	0.9525	2.1292	0.3556	0.2336	0.3556	0.2336
0.2	0.1	0.69331	2.27404	0.6934	2.2742	0.3741	0.1983	0.3741	0.1983
0.3	0.1	0.5201	2.52862	0.5201	2.5283	0.3643	0.1644	0.3643	0.1644
0.5	0.1	0.32116	3.03519	0.3212	3.0351	0.3535	0.1564	0.3535	0.1564
0.1	0.2	0.50565	2.38182	0.5057	2.3817	0.3476	0.1457	0.3476	0.1457
0.1	0.3	0.25228	2.40995	0.2523	2.4099	0.3843	0.3072	0.3843	0.3072
0.1	0.5	0.05429	2.38353	0.0543	2.3834	0.3556	0.3426	0.3556	0.3426

in generating/degenerating chemical reaction parameter (Kr<0/ Kr>0) results an enhancement of the fluid velocity in the entire fluid flow, which results in an increment of the thickness of the boundary layer.

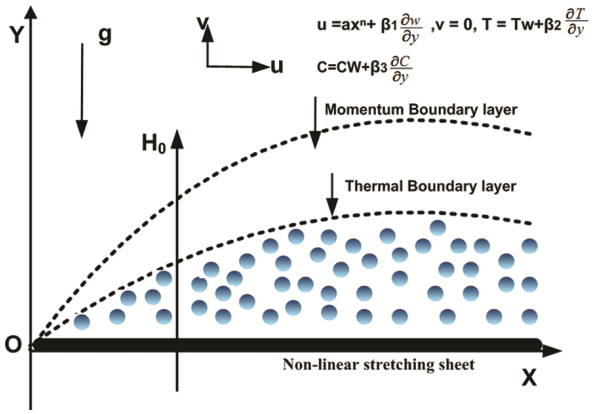

Fig. 1 – Sketch of the physical model.

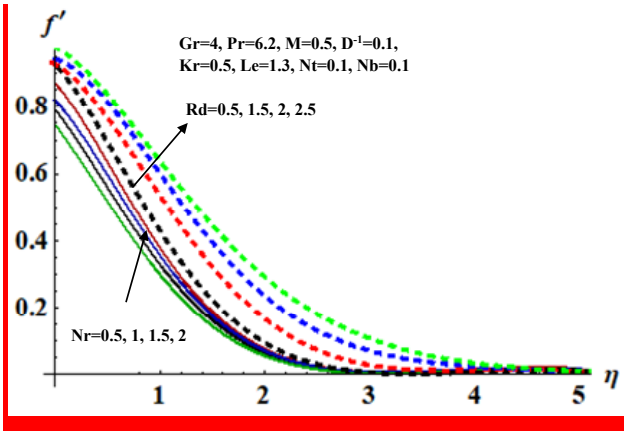

Fig. 2 – Effect of buoyancy ratio parameter (Nr) and radiation absorption (Rd) on *f ′ (η)*.

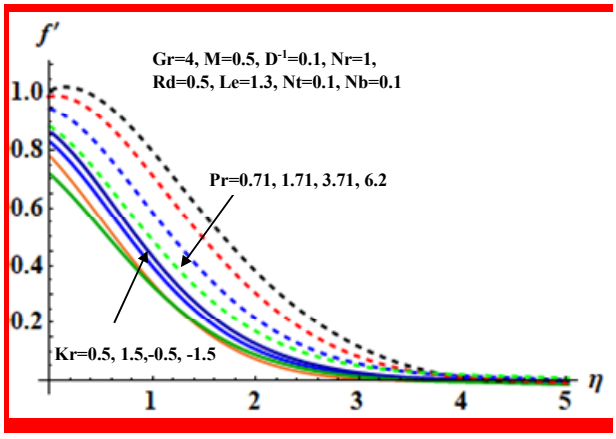

Fig. 3 – Effect of chemical reaction (Kr) and Prandtl number (Pr) on *f ′ (η)*.

5.2 Temperature profiles

Figure 4 depicts the effect of Nr and Rd on θ. With an increase in the values of Nr, depreciation in the temperature profiles is noticed. It leads to decrease in the thickness of the thermal boundary layer with increase in the higher values of Nr in the flow region, whereas a reverse effect is noticed with an increase on the values of Rd. Figure 5 represents the effect of Kr and Pr on temperature profile. It can be seen from the figure that a raise in the degenerating chemical reaction parameter increases the temperature, whereas, in the case of generating chemical reaction the temperature lessens. The temperature increases with the higher values of Pr in the boundary layer.

5.3 Nanoparticle concentration profiles

The impact of buoyancy ratio parameter Nr, radiation absorption Rd, chemical reaction Kr and Prandtl number Pr on nanoparticle concentration profiles φ are illustrated in Figs 6 and 7. Figure 6 illustrates the effect of Nr and Rd on φ. With increase in the values of Nr, a diminution in the nanoparticle

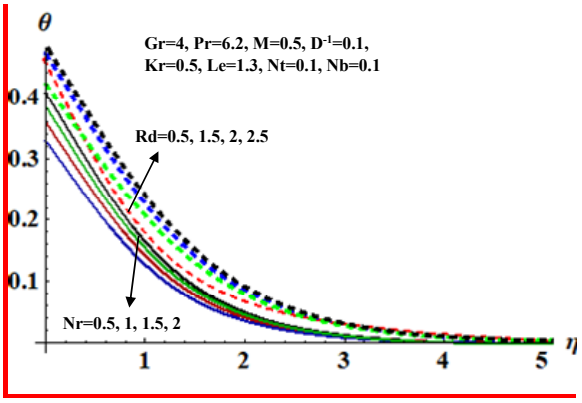

Fig. 4 – Effect of buoyancy ratio parameter (Nr) and radiation absorption (Rd) on *θ(η)*.

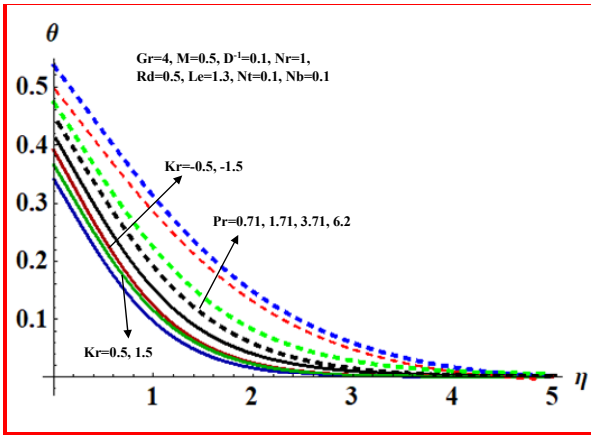

Fig. 5 – Effect of chemical reaction (Kr) and Prandtl number (Pr) on *θ (η)*.

concentration on the boundary layer is noticed, whereas a reversed effect is noticed in the case of Rd. The effect of Kr and Pr is illustrated in Fig. 7. From the figure, it can be explained that, a rise in the values of degenerating chemical reaction (Kr>0) parameter, the nanoparticle concentration reduces, whereas in both the case of generating chemical reaction (Kr<0) parameter the nanoparticle concentration enhances the boundary layer thickness. It can also have noted that the nanoparticle concentration enhances with higher values of Pr.

5.4 Skin friction, Nusselt number and Sherwood number

Figures 8-11 show the variations of the local skin friction coefficient $C_f (Re_x)^{1/2}$, local Nusselt number $Nu = (Re_x)^{-1/2}$ and local Sherwood number $Sh = (Re_x)^{-1/2}$ with different values of buoyancy ratio parameter Nr, radiation absorption Rd chemical reaction parameter Kr and Prandtl number Pr.

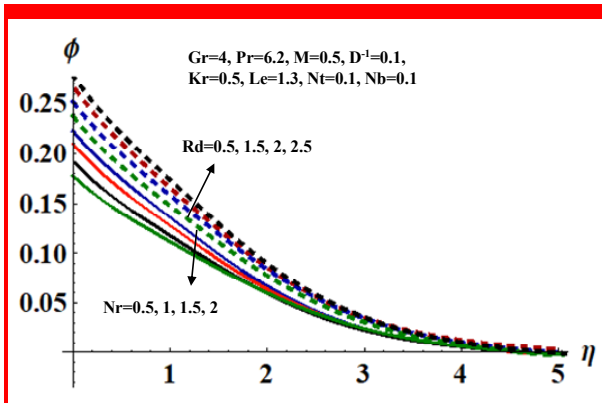

Fig. 6 – Effect of buoyancy ratio parameter (Nr) and radiation absorption (Rd) on *φ (η).*

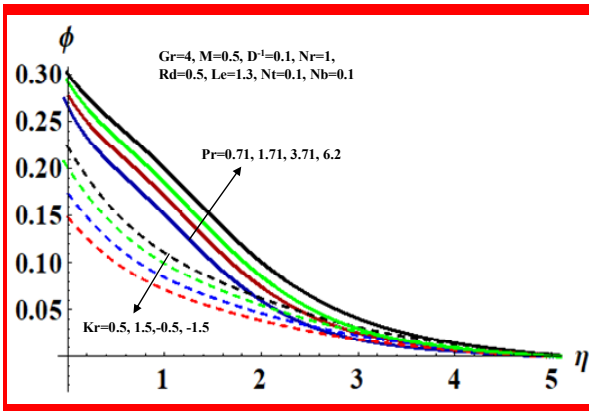

Fig. 7 – Effect of chemical reaction (Kr) and Prandtl number (Pr) on *φ (η).*

As displayed in Fig. 8, an increase in Nr and Rd causes depreciation in the skin friction variation coefficient. An enhancement in Nr and Rd, dimensionless velocity on the momentum boundary

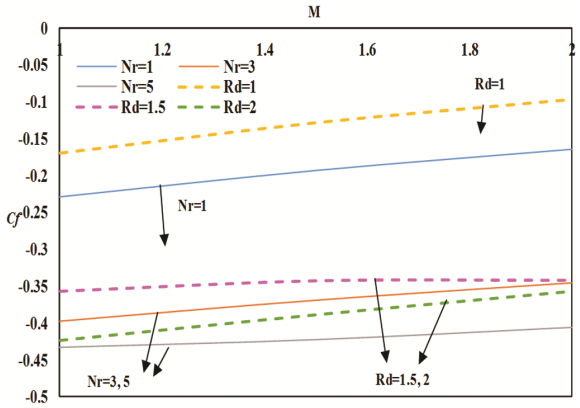

Fig. 8 – The variation of buoyancy ratio parameter (Nr) and radiation absorption (Rd) with skin friction coefficient (*Cf*) for Gr=4, M=0.5, Pr=6.2, D^{-1}=0.1, Le=1.3, N_t=N_b=0.1, n=2.

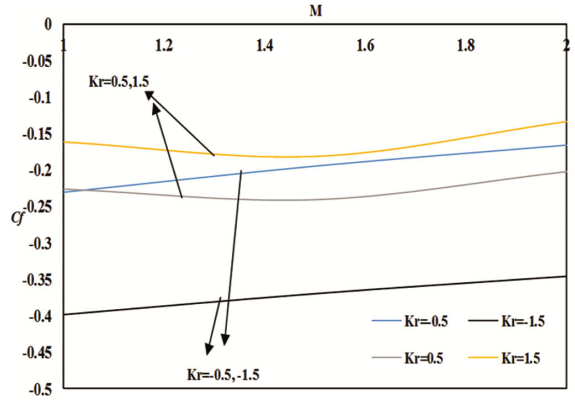

Fig. 9 – The variation of chemical reaction (Kr) with skin friction coefficient (*Cf*) for Gr=4, M=0.5, Pr=6.2, D^{-1}=0.1, Le=1.3, N_t=N_b=0.1, Nr=1 Rd=0.5, n=2.

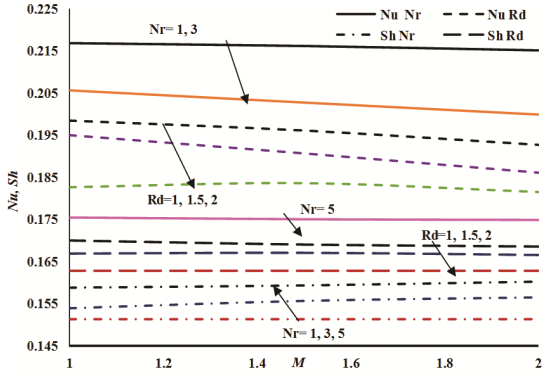

Fig. 10 – The variation of buoyancy ratio parameter (Nr) and radiation absorption (Rd) with Nusselt number (*Nu),* Sherwood number *(Sh)* for Gr=4, M=0.5, Pr=6.2, D^{-1}=0.1, Le=1.3, N_t=N_b=0.1, n=2.

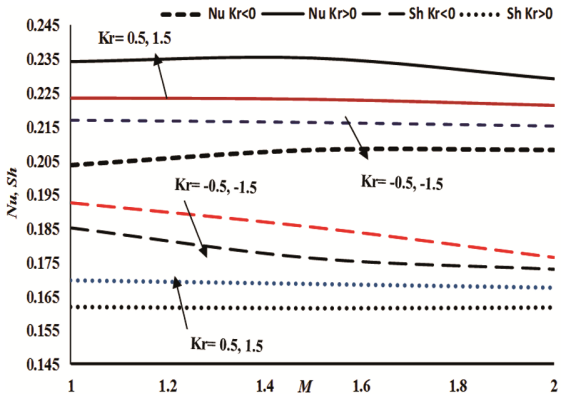

Fig. 11 – The variation of chemical reaction (Kr) with Nusselt number (*Nu),* Sherwood number *(Sh)* for Gr=4, M=0.5, Pr=6.2, D^{-1}=0.1, Le=1.3, N_t=N_b=0.1, Nr=1 Rd=0.5, n=2.

layer thickness gets enhanced on the surface of the stretching sheet. From Fig. 9, it can be noticed that the skin friction coefficient of the boundary layer reduces on the surface of the stretching sheet with an increase in the values of generating chemical reaction parameter (Kr<0). Interestingly, the skin friction coefficient increases with a rise in the values of degenerating chemical reaction parameter (Kr>0) and non-linear stretching sheet parameter *n*.

The variation of local Nusselt number Nu and Sherwood number Sh can be observed with different parametric values is illustrated in Fig. 10 and 11. The rate of heat transfer increases with an increase in Kr>0. This is due to the fact that the dimensionless temperature in the thermal boundary layer increases with an increase in Kr>0, non-linear stretching sheet parameter *n* in the presence of M, as a result the thickness of the thermal boundary layer becomes thicker on the stretching surface. The rate of heat transfer reduces with higher values of Nr, Rd and Kr<0 in the presence of M with non-linear stretching sheet parameter *n*. In the presence of M, the dimensionless temperature and the thermal boundary layer become thinner on the stretching sheet surface. Interestingly, from the profiles, Sh increases with an increase in the values of Nr and Kr>0. An increase in the values of Pr, Rd and Kr<0, the local Sherwood number reduces on the stretching surface. It is known that magnetic field reduces the flow of nanoparticle concentration within the boundary layer with increase in the values of Pr and Rd, which results into lesser mass transfer on the surface of the stretching sheet.

6 Conclusions

The steady, convective MHD two-dimensional boundary layer nanofluid flow past a non-linear stretching sheet is studied theoretically under the influence of radiation absorption and chemical reaction through porous medium. The effects of buoyancy ratio parameter Nr, radiation absorption Rd, chemical reaction Kr are analysed on the flow and heat and mass transfer characteristics with partial slip. The governing non-linear coupled boundary layer equations are solved using fifth order Runge-Kutta-Fehlberg method. The results show a significant effect of Grashof number, Hartmann number on the velocity and nanoparticle concentration distributions. The velocity and nanoparticle concentration increase on the surface of the stretching sheet due to the effect of the Lorentz force. The temperature and concentration distributions are augmenting with higher values of Rd, Nr and diminishing with Kr. However, the rate of heat transfer diminishes with larger values of Rd, Kr, Nr. The mass transfer increases with the higher values of Nr and Kr>0, whereas less mass transfer occurs due to the higher values of Pr, Rd and more mass transfer takes place with Kr<0. The skin friction coefficient enlarges with the higher values of Prand Kr>0, whereas a reverse effect is noted for higher values of Nr and Kr<0. It can be concluded that the values of temperature and nanoparticle concentration profiles in this work are much higher than those arose in the linear stretching sheet. By introducing varying proportions of temperatures between the surface and the nanofluid, a significant effect is noticed on the heat transfer characteristics and mass transfer distributions in the flow regions over a non-linear stretching sheet. This study is relevant to electromagnetic nanomaterial manufacturing processes and also high heat exchanging chemical engineering systems utilising magnetized nanofluids.

References

1 Choi S U S, *Int Mech Eng Congress Exposition*, 66 (1995) 99.
2 Brewster M Q, *Thermal radiative transfer properties*, (Wiley: New York), 1972.
3 Kuznetsov A V & Nield D A, *Int J Therm Sci*, 49 (2010) 243.
4 Buongiorno J, *ASME J Heat Transfer*, 128 (2006) 240.
5 Khan W A & Pop I, *Int J Heat Mass Transfer*, 53 (2010) 2477.
6 Van Gorder R A, Sweet E & Vajravelu K, *Commun Nonlinear Sci Numer Simul*, 15 (2010) 1494.
7 Hassan M, Tabar M M, Nemati H, Domairry G & Noori F, *Int J Therm Sci*, 50 (2011) 2256.
8 Akyildiz F T, Bellout H, Vajravelu K, Van Gorder R A, *Nonlinear Anal Real World Appl*, 12 (2011) 2919.
9 Rana P, Bhargava R, *Commun Nonlinear Sci Numer Simul*, 17 (2012) 212.
10 Das K, *J Egypt Math Soc*, 23 (2015) 451.

11 Sreedevi G, Rao R R, Prasada Rao D R V & Chamkha A J, *Ain Shams Eng J*, 7 (2016) 383.
12 Sreedevi G, Prasada Rao D R V, Makinde O D & Reddy G V R, *Indian J Pure Appl Phys*, 55(8) (2017) 551.
13 Makinde O D & Animasaun I L, *Int J Therm Sci*, 109 (2016) 159.
14 Sreedevi G, Prasada Rao D R V & Makinde O D, Multidiscipline Modeling in Materials and Structures, Emerald Publications, https://doi.org/10.1108/MMMS-06-2017 1573-6105.
15 Sreedevi P, Reddy P S & Chamkha A J, *Powder Technol*, Elsevier, 315 (2017) 194.
16 Jahan S, Sakidin H, Nazar R & Pop I, *J Mol Liquids*, 233 (2017) 211.
17 Dharmendar Reddy Y, Srinivasa Rao V, Ramya D & Anand Babu L, *Am Sci Pub*, 7 (2018) 404.
18 Sakiadis B C, *Am Inst Chem Eng*, 7 (1961) 26.
19 Crane L J, *Z Angew Math Phys*, 21 (1970) 645.
20 Schlichting H, *Boundary-layer theory*, (McGraw-Hill: New York), 1955.
21 Grubka L G & Bobba KM, *ASME J Heat Transfer*, 107 (1985) 248.
22 Cortell R, *Appl Math Comput*, 170 (2005) 706.
23 Ishak, Nazar R & Pop I, *Meccanica*, 44 (2009) 369.
24 Wang C Y, *Nonlinear Anal Real World Appl*, 10 (2009) 375.
25 Abbasbandy S, Ghehsareh H R & Hashim I, *UPB Sci Bull Ser A*, 74 (2012) 47.
26 Noghrehabadi A, Pourrajab R & Ghalambaz M, *Int J Therm Sci*, 54 (2012) 253.
27 Prasad K V, Datti P S, Vajravelu K, *J King Saud Univ Sci*, 25 (2013) 313.
28 Goyal M & Bhargava R, *ISRN Nanotechnol*, (2013) Article ID 931021.
29 Cortell R, *J King Saud Univ Sci*, 26 (2014) 161.
30 Sheikholeslami M, Ellahi R, Ashorynejad H R, Donairry G & Hayat T, *J Comput Theor Nanosci*, 11 (2014) 486.
31 Khalili S, Dinarvand S, Hosseini R, Tamim H & Pop I, *Chin Phys B*, 23 (2014) 04.
32 Zaim K, Ishak A & Pop I, *Sci Rep*, 4 (2014) 4404.
33 Seth G S, Kumbhakar B & Sarkar S, *J Nat Sci Sustain Technol*, 8 (2014) 273.
34 Hayat T, Imtiaz M & Alsaedi A, *Appl Math Mech Engl*, 36 (2015) 1513.
35 Mabood F, Khan W A & Ismail A I M, *J Magn Magn Mater*, 374 (2015) 569.
36 Seth G S, Sharma R, Kumbhakar B & Chamka A J, *Eng Comput*, 33 (2016) 907.